BOLETIN DE LA SOCIEDAD ESPAÑOLA DE
Cerámica y Vidrio
www.elsevier.es/bsecv

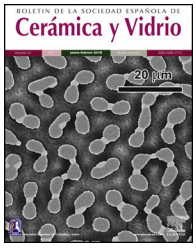

Effects of shell-thickness on the powder morphology, magnetic behavior and stability of the chitosan-coated Fe_3O_4 nanoparticles

Pablo Arévalo-Cid[a,*], *Josefa Isasi*[a], *Amador C. Caballero*[b], *Fátima Martín-Hernández*[c,d,e], *Ramón González-Rubio*[f]

[a] *Departamento de Química Inorgánica, Facultad de Ciencias Químicas, Universidad Complutense de Madrid, Ciudad Universitaria s/n, 28040 Madrid, Spain*
[b] *Departamento de Electrocerámica, Instituto de Cerámica y Vidrio (CSIC), Kelsen 5, 28049 Madrid, Spain*
[c] *Departamento de FTAA I, Facultad de Ciencias Físicas, Universidad Complutense de Madrid, Ciudad Universitaria s/n, 28040 Madrid, Spain*
[d] *Instituto de Geociencias (UCM, CSIC), 28040 Madrid, Spain*
[e] *Instituto de Magnetismo Aplicado (UCM), 28230 Las Rozas, Spain*
[f] *Departamento de Química Física I, Facultad de Ciencias Químicas, Universidad Complutense de Madrid, Ciudad Universitaria s/n, 28040 Madrid, Spain*

ARTICLE INFO

Article history:
Received 24 September 2020
Accepted 22 December 2020
Available online 11 January 2021

Keywords:
Chitosan
Magnetic nanocomposites
Superparamagnetism
Suspension stability
Aggregation

ABSTRACT

Chitosan-coated Fe_3O_4 nanoparticles were prepared by coprecipitation followed by reaction with chitosan and different volumes of glutaraldehyde. Coating was modified by varying the volume of glutaraldehyde and reaction time. XRD pattern shows maxima compatible Fe_3O_4 structure. FTIR spectroscopía confirms the presence of chitosan, more evident in samples with higher chitosan content, as denoted by TGA. TEM images of samples with low glutaraldehyde content reveal particles coated with a homogeneous chitosan shell. Meanwhile, those prepared with high glutaraldehyde volume show nanoparticles dispersed in an organic matrix. Samples present almost superparamagnetic behavior with magnetization saturation values that are reduced as the content of organic matter increases. Regarding the stability of these samples in solution, the presence of a homogeneous coating improves the initial suspension, although it does not prevent its subsequent aggregation over time. However, this aggregation process is reduced for sample synthesized with 1 mL of glutaraldehyde after 6 h of reaction.

* *Corresponding author.*
E-mail address: pabloarevalo@ucm.es (P. Arévalo-Cid).
https://doi.org/10.1016/j.bsecv.2020.12.001

Efecto del espesor del recubrimiento en la morfología del polvo, el comportamiento magnético y la estabilidad de nanopartículas de Fe_3O_4 recubiertas con quitosano

Palabras clave:
Quitosano
Nanocomposites magnéticos
Superparamagnetismo
Estabilidad en suspensión
Agregación

RESUMEN

Se han preparado nanopartículas de Fe_3O_4 recubiertas con quitosano mediante coprecipitación seguida de reacción con quitosano y diferentes volúmenes de glutaraldehído. El recubrimiento fue modificado a través de la variación del volumen de glutaraldehído y el tiempo de reacción. Los patrones de DRX muestran máximos compatibles con la estructura del Fe_3O_4. La espectroscopía IRTF confirma la presencia de quitosano, que se hace más evidente para muestras con altos contenidos de quitosano, como se observa mediante ATG. Las imágenes de MET con volumenes pequeños de glutaraldehído revelan partículas recubiertas homogéneamente con una coraza de quitosano. Por su parte, aquellas preparadas con grandes cantidades exhiben nanopartículas dispersas en la matriz orgánica. Las muestras presentan un comportamiento prácticamente superparamagnéticos con valores de magnetización a la saturación que se reducen cuanto mayor es le contenido de materia orgánica. Atendiendo a la estabilidad de las muestras en disolución, la presencia de un recubrimiento homogéneo mejora la suspensión inicial del material, pero no previene la agregación con el tiempo. Sin embargo, este proceso de agregación se ve reducido para la muestra sintetizada con 1 ml de glutaraldehído con un tiempo de reacción de 6 horas.

Introduction

Over the years, the preparation of magnetic nanoparticles of two of the most common forms of iron oxides, magnetite (Fe_3O_4) and maghemite (γ-Fe_2O_3) has been the subject of great interest by scientists on the basis to its numerous technological applications. Among them, we can mention magnetic resonance imaging [1,2], hyperthermia [3,4], targeted drug delivery [5,6], biosensing [7,8] and adsorption of heavy metal ions [9–11] or organic pollutants [12].

Nanoparticles of Fe_3O_4 or γ-Fe_2O_3 oxides smaller than 15 nm offer unique advantages over other materials. Among them, they can be synthesized by low-cost methods, are physically and chemically stable, biocompatible, non-toxic [13], present strong magnetic saturation and superparamagnetism at room temperature, which means that these nanoparticles can be temporarily magnetized in the presence of an external magnetic field with disappearance of the magnetization upon field removal [14,15]. Attending to its higher magnetization saturation value, based on its usefulness as a magnetic material capable of responding to an external magnetic field [16], Fe_3O_4 phase has been selected as the base of the research in this paper.

A variety of preparation methods based on aqueous and non-aqueous routes have been reported in the literature for the synthesis of Fe_3O_4 or γ-Fe_2O_3 nanoparticles as chemical coprecipitation [17,18], thermal decomposition [19,20], solvothermal synthesis [21,22] or sol–gel [23]. Depending on the method of synthesis used, the morphology of the powder and the size of the constituent particles will be affected and, ultimately, this will also influence the magnetic behavior of the prepared sample. At this point, it should be noted that coprecipitation method has advantages such as experimental simplicity, mild reaction conditions, relatively short reaction time and the use of water as a solvent [24].

On the other hand, it should be considered that once the nanoparticles of Fe_3O_4 or γ-Fe_2O_3 are obtained, these nanoparticles have hydrophobic surfaces with a large surface area to volume ratio in the absence of any surface coating material [25–27]. These particles agglomerate to form large clusters due to hydrophobic interactions between the particles, resulting in increased relative particle size of the cluster. To prevent the aggregation, a stabilizer of the nanoparticles, as a surfactant or a polymer, is usually added during the preparation. Dispersing agents such as oleic acid or oleylamine can perform a double function: control the growth of particles and prevent their aggregation [25–27]. In addition, a high-density coating is often implemented as an alternative strategy to stabilize iron oxide nanoparticles.

Magnetic nanoparticles can be coated using different inorganic and polymeric shells [24,28,29]. When preparing a compound suitable for application in biomedicine or removal of heavy metal ions, various types of materials such as silica [28,30], biomolecules [31,32], Au or Ag pure [33,34] and polymer [35–37] have been investigated as surface modifiers of iron oxide nanoparticles. Among them, natural biopolymers are favored due to their high biocompatibility and biodegradability [38,39]. Chitosan is a polysaccharide obtained by deacetylation of chitin, a polymer that is part of the external skeletons of many crustaceans and, therefore, one of the most abundant in nature [40]. Its cationic character is the differential point of other natural polymers, which in most cases are neutral or anionic macromolecules. The presence of free amino groups gives it the possibility of a subsequent functionalization. In this sense, chitosan can be incorporated either as a nanoparticle shell in a core–shell structure or act as a polymer matrix into which the magnetic material can

be embedded. Focusing on the first process, which is the object of the research described here, it should be noted that multiple parameters could affect the stability of the chitosan cover around the magnetic nanoparticle. For this reason, the improvement of core–chitosan shell structures with chitosan has been reported in the literature using various chemical cross-linking processes [41,42]. Aldehydes such as glyoxal or glutaraldehyde have been commonly used to cross-link the chitosan chains by their reaction with the amino groups to form imines. These bonds modify the final properties of the materials prepared, determining their mechanical strength or their behavior in aqueous media. In fact, once the iron oxide coated nanoparticles are obtained, their environmental and public health impact will depend largely on how stable these particles suspended in the natural environment.

Based on the above considerations, results describing the preparation of chitosan-coated Fe_3O_4 samples are presented here. Some similar studies have been carried out, however, from our knowledge, in none of them is a study so broad and systematic that it also addresses the stability of this type of samples in aqueous solutions. A two-stage process, chitosan-coated Fe_3O_4 nanoparticles were prepared by varying the volume of glutaraldehyde and by increasing chitosan reaction time for the same glutaraldehyde content. The effects of the different chitosan thicknesses on the structural features, powder morphology, magnetic properties and stability of samples in solutions were evaluated.

Experimental

Preparation of Fe_3O_4 sample by coprecipitation

For the preparation of samples of the same composition, precursor agents ($FeCl_3{\cdot}6H_2O$ and $FeCl_2{\cdot}4H_2O$) in a 2:1 ratio were dissolved in 150 mL of deionized water in argon atmosphere. The resulting solution was taken into a glass reactor under both mechanical stirring and argon flow. This flow provides an inert atmosphere that avoids the presence of oxygen in the reaction that would allow the formation of maghemite (γ-Fe_2O_3) or hematite (α-Fe_2O_3) as secondary phases. In addition, to achieve an alkaline reaction medium, 20 mL of 25% NH_3 was added, detecting a color change of the solution from blood red to black by formation of iron hydroxides. The reactor was connected to a thermal water bath warming up to 75 °C, being stirred for 30 min. Then, 1 mL of oleic acid (OA) is added to favor the dispersion of nanoparticles [43,44] and the reaction system was maintained under mechanical stirring for 1 h. A solid black powder was obtained, which was separated from the liquid by magnetic decantation and was washed several times with a mixture of ethanol/water, drying finally in a stove at 50 °C.

Preparation of chitosan-coated Fe_3O_4 samples

0.125 g of previously synthesized Fe_3O_4 sample, dispersed with 0.5 mL of oleic acid (OA) and mixed with 0.25 g of commercial chitosan (Sigma-Aldrich, Medium molecular weight, 75–85% deacetylated) in 50 mL of 2.0 wt% acetic acid solution was poured into a beaker and stirred using an ultrasonic bath for 20 min. As is known, the acid medium favors the solubility of chitosan [45] and its interaction with the Fe_3O_4 powder by the protonation of the amino groups present in the chitosan [46]. The resulting mixtures were poured in a glass reactor, being stirred for 20 min and heated to 40 °C. In order to induct a crosslinking reaction, different volumes of glutaraldehyde (GA) (25% by weight) were added (0, 0.5, 0.75, 1, 1.5 and 2 mL) on prepared solutions as described above. Aldehyde groups from GA react with amine moieties of chitosan, leading to crosslinked polymer chains. All reactions with GA were carried out for 3 h.

In a parallel study, different chitosan-coated Fe_3O_4 samples were prepared by adding 1 mL of GA, but now varying the reaction time of Fe_3O_4 sample with chitosan at 6 and 12 h.

In all cases, gray color powders were isolated from the liquid by magnetic decantation and they were washed several times with a mixture of deionized water and ethanol. Subsequently, they were dried in an oven at 50 °C.

Characterization

The different prepared samples of Fe_3O_4 composition were characterized by X-ray diffraction (XRD) employing an X'Pert-MPD Philips diffractometer with Cu Kα radiation. A step scan of 0.04° (2θ) in the range 10–70° and a counting time of 1 s for each step were employed for data collection. Chitosan and Fe_3O_4 associations were evaluated by using Fourier-transform infrared spectroscopy (FTIR). Spectra were recorded on a Prestige-21 Fourier-transform spectrophotometer using the KBr pellet technique within the (4000–400) cm^{-1} range. To prove the encapsulation efficiency and the thickness of the coatings, transmission electron microscopy (TEM) images were obtained on a JEOL 2100F transmission electron microscope, operating at 200 kV and equipped with a field emission electron gun providing a point resolution of 0.19 nm. For TEM observations, the powders were dispersed in n-butanol and drops of the corresponding suspensions were deposited on carbon-coated copper grids. The stability of the synthesized covered samples with respect to heating in the presence of air was evaluated from thermogravimetric analysis, recorded on TGA Q50 (TA Instruments). The run was carried out in air at a heating rate of 10 °C/min. M–H curves were registered in a coercivity spectrometer developed by the University of Kazan (Coercivity Spectrometer J-meter) [47]. Finally, the suspension stability of the chitosan-coated Fe_3O_4 samples and their aggregation capacity over time were analyzed by dynamic light scattering (DLS) experiments using a Zetasizer Nano ZS (Malvern Instruments Ltd., Worcestshire, UK). All the DLS measurements were performed at 25 °C using as radiation the red line (wavelength, $\lambda = 632$ nm) of a He–Ne laser.

Results and discussion

Structural characterization

Fig. 1 shows the XRD patterns of the Fe_3O_4 synthesized sample. All observed reflections can be indexed to a cubic symmetry of space group $Fd\bar{3}m$ with $Z = 8$, compatible with an inverse spinel-type structure, characteristic of Fe_3O_4 [ICDD 82-1533].

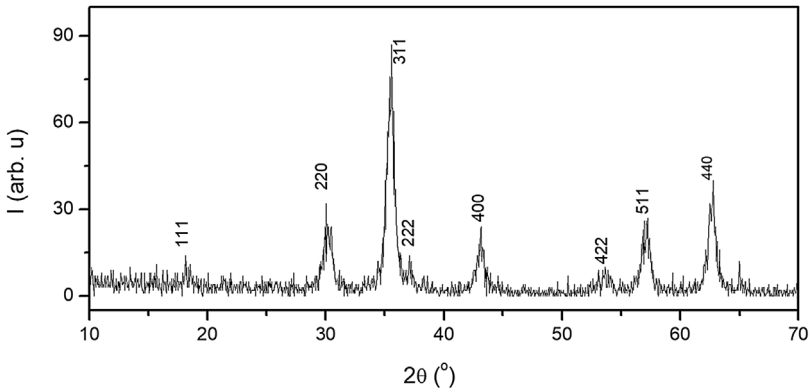

Fig. 1 – XRD pattern of the Fe_3O_4 sample.

XRD data were analyzed by the Rietveld method using the FULLPROF program and, the results, which we published in previous work [48], finding a cell parameter $a = 8.3781(5)$ Å. The result highlights the existence of 95% of the magnetite phase together with 4.7% of the maghemite phase and, therefore, partial oxidation of the sample thus synthesized.

An estimation of the average crystalline size of the as-synthesized sample using the Scherrer formula [49]. The diffraction maxima used for the calculation were (2 2 0), (3 1 1), (5 1 1 and (4 4 0). It was found a value of 11.5 nm in size for prepared the nanoparticles. This particle size is of the same order as determined in samples of the same composition prepared by the same synthesis method [50–52].

Fig. 2 shows the FTIR spectra of Fe_3O_4 sample, pure chitosan and chitosan-coated Fe_3O_4 samples for $x = 0$, 0.5, 0.75, 1, 1.5 and 2 mL of glutaraldehyde volume. In the spectrum of Fe_3O_4 sample, a high-intensity band can be observed at about 600 cm^{-1} assignable to intrinsic stretching vibration of Fe—O bonds located at tetrahedral site of the inverse spinel structure type of this oxide [53]. This band is also present in the spectra of the coated samples. In the rest of the spectrum, a broad band with a maximum close to 3400 cm^{-1}, probably attributable to the O—H stretching of water adsorbed on the surface of these materials, can be observed and another band at 1630 cm^{-1} also assignable to the H_2O bending vibrations of water adsorbed. The band at 3376 cm^{-1} are related with the presence of O—H groups from water or rests of free. The bands 2920–2850 cm^{-1} were attributed to asymmetric and symmetric CH_2 stretching of the oleic acid, which remains in nanoparticles surface. It is also reflected by the presence of the band at 1615 cm^{-1}, associated with C=C double bonds, with a wide shape due to the appearance in this area of the signal of O—H bending band. The doublet appearing at 1452 and 1523 cm^{-1} correspond to the asymmetric and symmetric stretching vibrations of the carboxyl group when is coordinated to the surface as carboxylate ($—COO^-$) [54,55].

In the chitosan pure spectrum, characteristic bands of its functional groups are also observed: bands at 1664 and 1562 cm^{-1} are assignable to the O—H flexion, the band at 1380 cm^{-1} to the flutter of CH_2 while the bands at 1076 cm^{-1} were attributed to C—O and C—O—C bonds [56]. All these bands appear somewhat displaced in the spectra of chitosan-coated Fe_3O_4 samples, which may indicate the possible association of chitosan and Fe_3O_4 sample. This effect has been previously observed and described by Long et al. [57].

Spectra of samples synthesized with increasing GA volumes show bands that are visualized in spectra of pure chitosan and Fe_3O_4 sample. In the spectrum of the sample prepared by the addition of 2 mL of GA an additional band at 1712 cm^{-1} also appears, which can be assigned to the strain C=O bond and related to the high percentage of glutaraldehyde present [58].

Thermogravimetric analysis (TGA)

The thermal stability on air of all synthesized samples was evaluated from the thermogravimetric analysis. TGA/DTA curves of chitosan-coated Fe_3O_4 samples prepared with GA volume variation and increasing the reaction time are shown in Fig. 3a and b, respectively, where a weight loss below 150 °C is found due to the adsorbed water on the surface. In addition, a significant weight loss between 150 and 400 °C can be also observed. In fact, while in TGA curve of sample prepared without glutaraldehyde (0 mL) a loss of mass by decomposition at lower temperatures is seen, in TGA curve of sample that contain the greatest amount of crosslinking agent (2 mL) these losses are caused by combustion of the organic layer and takes place gradually until it reaches 600 °C. These results are in accordance with those described elsewhere [59,60]. Chitosan begins to decompose approximately at 200 °C, although weight losses also observed at temperatures above 500 °C when the chitosan is crosslinked with glutaraldehyde. In TGA/DTA curves of samples prepared with low content of GA, the weight loses determined is close to 10%, increasing progressively from 8.88% (for 0 mL of GA) to 8.90 (0.5 mL of GA), 9.34 (0.75 mL of GA) and 10.70% (1 mL of GA). For chitosan-coated Fe_3O_4 samples prepared with a large amount of glutaraldehyde, exist an excessive weight loss (68.35% for 1.5 mL of GA and 90.88% for 2 mL of GA). These losses increase gradually in TGA of chitosan-coated Fe_3O_4 samples prepared with 1 mL of GA and increasing the chitosan reaction time (see Fig. 3b) (10% for 3 h, 11.6% for 6 h and 12.6% for 12 h).

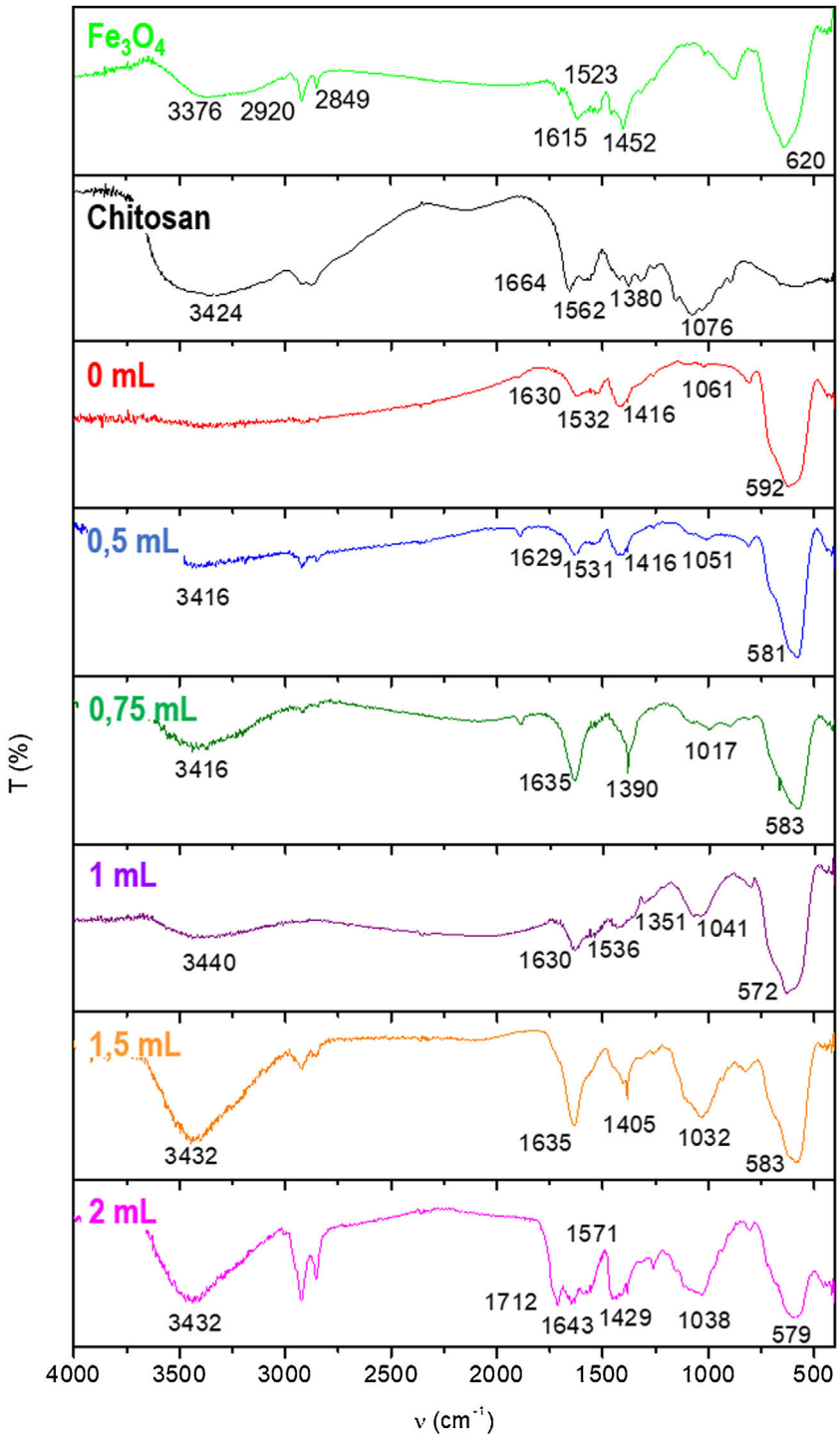

Fig. 2 – FTIR spectra of Fe_3O_4 sample, pure chitosan and Fe_3O_4@chitosan synthesized with the addition of different glutaraldehyde volumes.

Transmission electron microscopy (TEM)

TEM images of Fe_3O_4 and chitosan-coated Fe_3O_4 samples are shown in Fig. 4. Size calculations were made by using the ImageTool software, measuring at least 80 particles for every sample. TEM image of Fe_3O_4 sample (Fig. 4a) reveals spherical particles with an average diameter of 11.8 nm. This result is in good agreement with the average size calculated by XRD. A similar arrangement of nanoparticles can be seen in TEM images of chitosan-coated Fe_3O_4 samples prepared with low content of glutaraldehyde (0, 0.5 and 0.75 mL) with a lower powder aggregation, although these nanoparticles are now coated with a homogeneous and thin chitosan shell of 1.2–1.3 nm. This thin shell would justify the similar losses of organic matter determined from TGA curves. TEM image of the chitosan-coated Fe_3O_4 sample prepared with 1 mL of

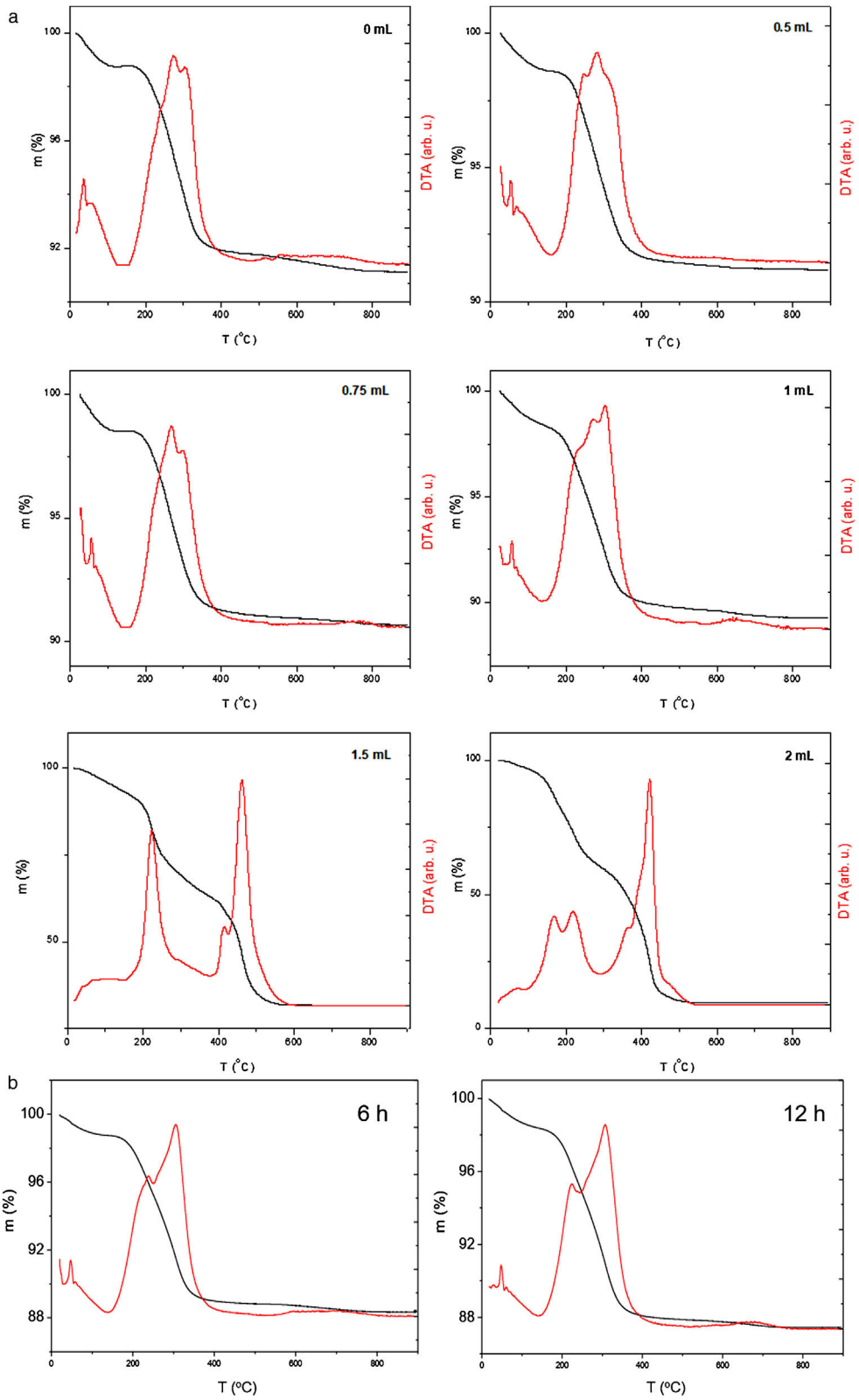

Fig. 3 – (a) TGA (black) and DTA (red) curves of Fe_3O_4–chitosan samples prepared with different glutaraldehyde volumes. (b) TGA (black) and DTA (red) curves of Fe_3O_4–chitosan samples prepared with 1 mL of glutaraldehyde.

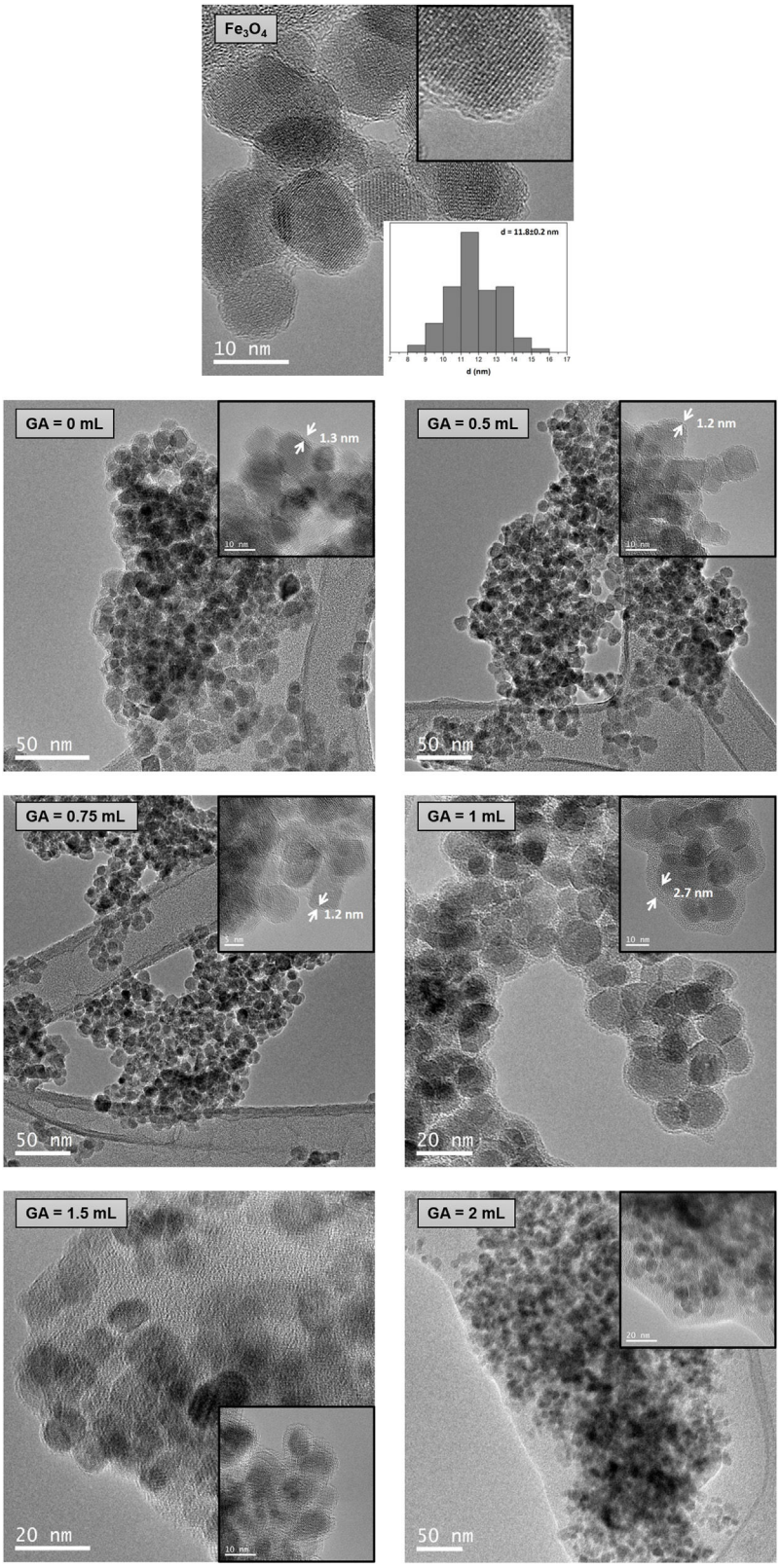

Fig. 4 – TEM image of Fe_3O_4 sample and distribution of average particle size and TEM images of Fe_3O_4–chitosan samples prepared with different GA volumes.

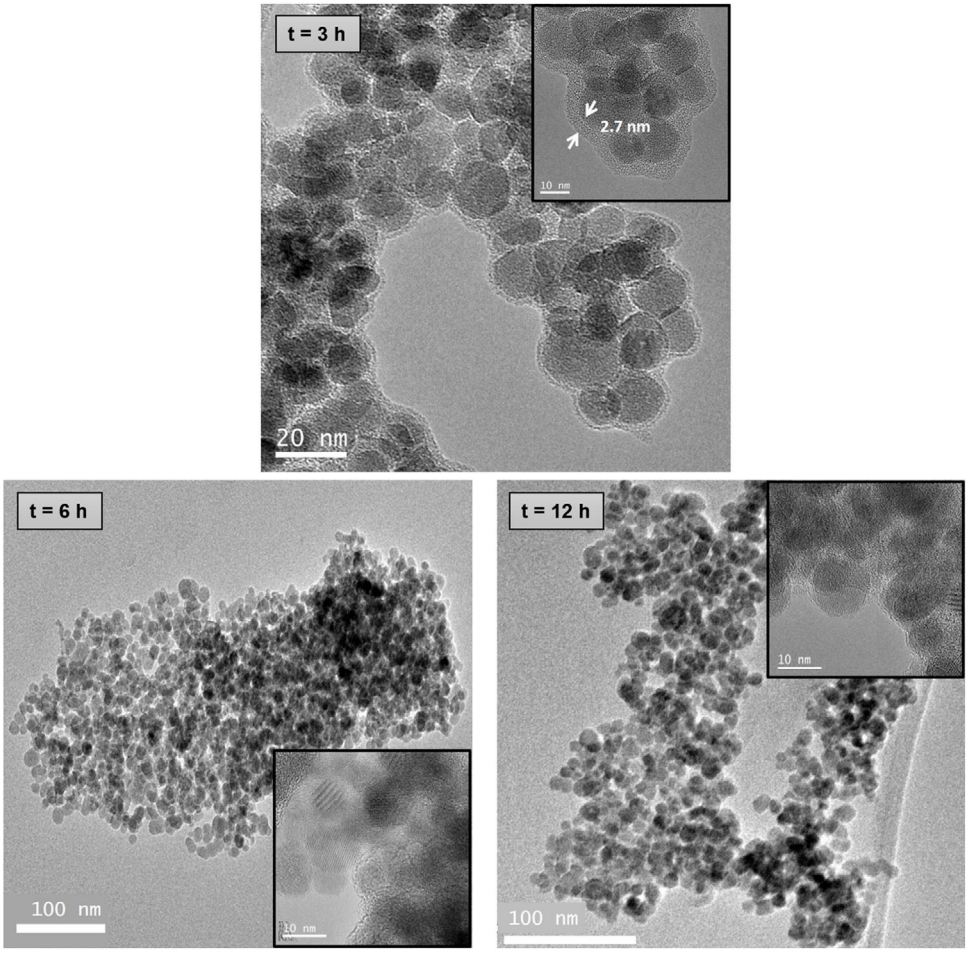

Fig. 5 – TEM images of Fe_3O_4–chitosan nanocomposites prepared with 1 mL of GA.

GA shows nanoparticles surrounded by a chitosan shell of 2.7 nm. The thickness has increased and this result is in good agreement with the high organic content determined by TGA analysis (10.70%) in this sample. By contrast, several amorphous zones are seen in TEM images of the chitosan-cover Fe_3O_4 samples prepared with 1.5 and 2 mL of GA, which cannot be considered as coating of the Fe_3O_4 nanoparticles surface and, therefore, the excess polymer seems to act as an organic matrix where the Fe_3O_4 nanoparticles are dispersed. These results are in good agreement with the high organic content determined by TGA (68.35% and 90.88% for samples prepared with 1.5 and 2 mL of GA, respectively).

TEM images of chitosan-coated Fe_3O_4 samples prepared with 1 mL of GA and increasing the chitosan reaction time (3, 6 and 12 h) are shown in Fig. 5. As the reaction time increases from 6 to 12 h, also Fe_3O_4 nanoparticles dispersed in an organic matrix can be seen here. These results indicate that an increase in the reaction time with chitosan does not favor the process of coating the nanoparticles and if the segregation of excess organic.

Magnetic behavior

The magnetic field dependence of magnetization at room temperature of all synthesized sampled is presented in Fig. 6. Table 1 summarizes the magnetic parameters determinates from these representations.

Fe_3O_4 sample and chitosan-coated Fe_3O_4 samples show a practically superparamagnetic behavior with very low coercive fields (between 8 and 14 Oe) and M_r values (between 1.99 and 0.19 emu/g). On the other hand, it can be observed that Fe_3O_4 sample presents a reduction of the saturation magnetization values (M_s = 67.48) with respect to the theoretical value of bulk magnetite (92 emu/g) [61]. This result can be explained by both the partial oxidation, as it was found in XRD experiments, and the canted spin on the surface of this kind of nanoparticles, which results in a non-contribution of its magnetic moment to total magnetization [62]. A reduction of M_s is evidenced with the chitosan cover with respect to the value of the uncoated sample, Table 1. The non-magnetic character of chitosan and its content makes possible the noticeable reduction of M_s. Much more evident for the samples prepared with greater GA content (1.5 and 2 mL) that have a higher chitosan content. These results are in good agreement with that reported by Freire et al. among others [63–65], with the percentages determined from TGA curves and with the powder morphology observed in the TEM images of Fig. 5.

For chitosan-coated Fe_3O_4 samples prepared with 1 mL of GA with increasing the reaction time, can be also observed a slight reduction of M_s, in good agreement with the contents

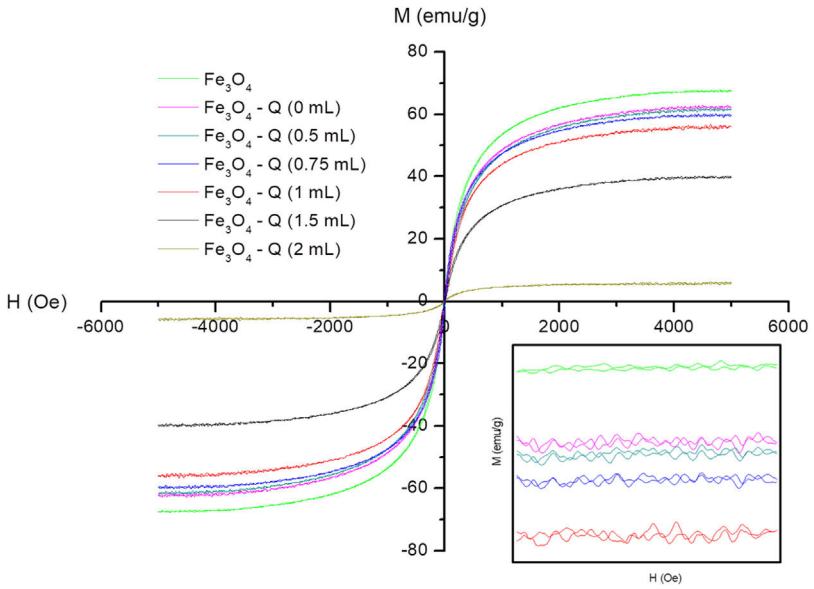

Fig. 6 – *M vs H* loops (300 K) of Fe_3O_4 and Fe_3O_4–chitosan samples prepared with different GA volumes.

Table 1 – Magnetic parameters of prepared samples.

Samples	V_{GA} (mL)	*t* (h)	M_s (emu/g)	M_r (emu/g)	H_c (Oe)
Fe_3O_4	0.00	0	67.48	1.99	14
Fe_3O_4–Q	0.00	3	61.21	1.39	9
	0.50	3	62.50	1.28	9
	0.75	3	59.61	1.79	8
	1.50	3	39.92	0.92	9
	2.00	3	5.77	0.19	10
	1.00	3	56.14	1.50	13
	1.00	6	55.04	1.23	9
	1.00	12	53.54	1.35	8

determined by TGA. In summary, the decrease of M_s is a multiple source phenomenon that depends on the GA concentration and reaction time, being the first the parameter that influences most of the experiment carried out.

Dynamic light scattering (DLS)

Once the Fe_3O_4 and chitosan-coated Fe_3O_4 samples are obtained, their environmental and public health impact will depend largely on how stable these particles suspended in the natural environment. For this reason, we analyze in this work the effect of chitosan shell-thickness on the aggregation capacity of nanoparticles. It is noted that the absence of charge in the chitosan under the conditions of measurement (neutral pH) prevents the electrostatic repulsion of the nanoparticles with each other and the resulting colloidal stabilization for larger times [66].

Fig. 7 shows the hydrodynamic diameter evolution overtime for 0.01 g/L of distilled water for all synthetized chitosan-coated Fe_3O_4 samples. As a reference, the same variation for Fe_3O_4 sample suspended in water is also shown (black lines). An increase of the hydrodynamic size over time can be observed for the uncoated nanoparticles, which can be explained as a result of a process of aggregation *in situ*, generating aggregates with a minimum size of 175.4 nm. These aggregates are much larger than those determined by TEM for the corresponding nanoparticles. This fact reflects the tendency of the Fe_3O_4 sample to form nanoparticles aggregates over time due to its high surface/volume ratio, in good agreement with what has been described in the literature for particles of such size [67].

Larger values of hydrodynamic diameter are visualized in the chitosan-coated Fe_3O_4 samples prepared with GA = 0 and 0.5 mL. For these samples, the amount of chitosan is very low, favoring the aggregation process. In the chitosan-covered Fe_3O_4 samples prepared with GA = 1 and 2 mL, smaller size of the aggregate is initially observed. This phenomenon can be explained considering a better dispersion in water of samples as a result of the presence of chitosan. However, the observed evolution of hydrodynamic diameter over time is far from the linearity found for the Fe_3O_4 sample, giving rise to a curve that shows an increase of the size of the aggregates of nanoparticles that accelerate over time. The results of these studies found that the presence of a homogeneous chitosan coating improves the initial suspension of these samples, although they do not prevent the aggregation of constituent particles over time.

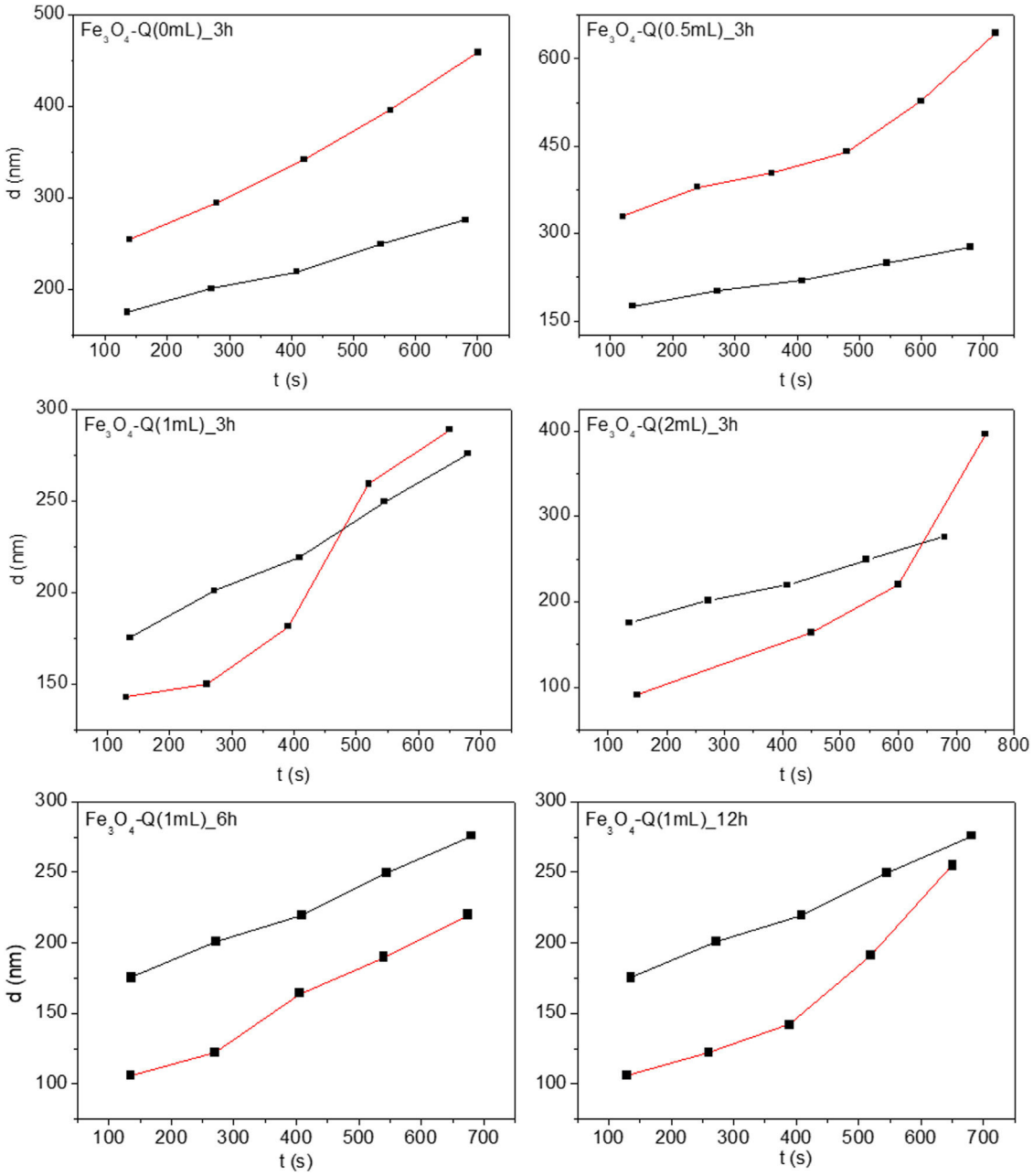

Fig. 7 – Dependence of hydrodynamic size overtime for some synthesized samples (variation for the Fe_3O_4 sample is shown by black lines).

The hydrodynamic diameter evolution over time for chitosan-coated Fe_3O_4 samples prepared with 1 mL of GA at different reaction times also suffers the equivalent aggregation phenomenon. However, the formation of nanoparticle aggregates seems to be reduced and even disappear in the sample obtained after 6 h of reaction with chitosan. In fact, TEM image of this sample (see Fig. 5) shows a homogeneous chitosan shell surrounding not a particle, but a group of nanoparticles of Fe_3O_4 of 12 nm. This fact leads to a reduction in surface/volume ratio, minimizing the surface energy, reducing aggregation and contributing to the stabilization of chitosan covered Fe_3O_4 nanoparticles in suspension. For this reason, this sample seems to be the most suitable for use in the natural environment.

Conclusions

The effects of the different chitosan thicknesses have been evaluated from the preparation of chitosan-coated Fe_3O_4 nanoparticles. X-ray patterns of Fe_3O_4 samples show reflections indexed to a cubic symmetry of space group $Fd\bar{3}m$ with $Z = 8$, compatible with an inverse spinel structure. FTIR spectra of synthesized samples evidence the presence of chitosan

which becomes more noticeable in samples with higher chitosan content and TGA curves show a significant weight loss which is the result of the combustion of the organic thickness. TEM images of chitosan-coated Fe_3O_4 samples synthesized with a lower GA volume show particles coated with a homogeneous chitosan shell of 1.2–1.3 nm. TEM images of samples synthesized with higher GA volume show dispersed nanoparticles in an organic matrix. The content of organic matter reduces the magnetization saturation values of these superparamagnetic samples. The presence of a homogeneous coating improves the suspension of the samples in solution, although it does not prevent their aggregation over time. However, this aggregation process seems to be reduced and even disappear for the sample synthesized with 1 mL of glutaraldehyde after 6 h of reaction with chitosan.

Funding

Fundación Neurociencias y Envejecimiento has supported this work through project 359/2014 as well as MINECO through the project MAT2016-80182-R.

REFERENCES

[1] E. Illés, M. Szekeres, E. Kupcsik, I.Y. Tóth, K. Farkas, A. Jedlovszky-Hajdú, E. Tombácz, PEGylation of surfacted magnetite core–shell nanoparticles for biomedical application, Colloid. Surf. A 460 (2014) 429–440.
[2] M.G.M. Schneider, M.J. Martin, D.F. Coral, D. Muraca, C. Gentili, M. Fernández van Raap, V.L. Lassalle, Selective contrast agents with potential to the earlier detection of tumors: insights on synthetic pathways, physicochemical properties and performance in MRI assays, Colloid. Surf. B 170 (2018) 470–478.
[3] M. Abdellahi, E. Karamian, A. Najafinezhad, F. Ranjbar, A. Chami, A. Khandan, Diopside-magnetite: a novel nanocomposite for hyperthermia applications, J. Mech. Behav. Biomed. 77 (2018) 534–538.
[4] E.M. Múzquiz-Ramos, V. Guerrero-Chávez, B.I. Macías-Martínez, C.M. López-Badillo, L.A. García-Cerda, Synthesis and characterization of maghemite nanoparticles for hyperthermia applications, Ceram. Int. 41 (2015) 397–402.
[5] H. Shagholani, S.M. Ghoreishi, M. Mousazadeh, Improvement of interaction between PVA and chitosan via magnetite nanoparticles for drug delivery application, Int. J. Biol. Macromol. 78 (2015) 130–136.
[6] V. Balan, G. Dodi, N. Tudorachi, O. Ponta, V. Simon, M. Butnaru, L. Verestiuc, Doxorubicin-loaded magnetic nanocapsules based on N-palmitoyl chitosan and magnetite: synthesis and characterization, Chem. Eng. J. 279 (2015) 188–197.
[7] A. Samphao, P. Butmee, P. Saejueng, C. Pukahuta, Ľ. Švorc, K. Kalcher, Monitoring of glucose and ethanol during wine fermentation by bienzymatic biosensor, J. Electroanal. Chem. 816 (2018) 179–188.
[8] D. Baratella, M. Magro, G. Sinigaglia, R. Zboril, G. Salviulo, F. Vianello, A glucose biosensor based on surface active maghemite nanoparticles, Biosens. Bioelectron. 45 (2013) 13–18.
[9] H. Li, X. Li, Y. Chen, J. Long, G. Zhang, T. Xiao, P. Zhang, C. Li, L. Zhuang, W. Huang, Removal and recovery of thallium from aqueous solutions via a magnetite-mediated reversible adsorption–desorption process, J. Clean. Prod. 199 (2018) 705–715.
[10] M. Karanac, M. Đolić, Z. Veličković, A. Kapidžić, V. Ivanovski, M. Mitrić, A. Marinković, Efficient multistep arsenate removal onto magnetite modified fly ash, J. Environ. Manage. 224 (2018) 263–276.
[11] L.B. Tahar, M.H. Oueslati, M.J.A. Abualreish, Synthesis of magnetite derivatives nanoparticles and their application for the removal of chromium (VI) from aqueous solutions, J. Colloid Interf. Sci. 512 (2018) 115–126.
[12] L. Mohammed, H.G. Gomaa, D. Ragab, J. Hu, Magnetic nanoparticles for environmental and biomedical applications: a review, Particuology 30 (2017) 1–14.
[13] L.H. Reddy, J.L. Arias, J. Nicolas, P. Couvreur, Magnetic nanoparticles: design and characterization, toxicity and biocompatibility, pharmaceutical and biomedical applications, Chem. Rev. 112 (2012) 5818–5878.
[14] C.P. Bean, J.D. Livingston, Superparamagnetism, J. Appl. Phys. 30 (1959) 120S–129S.
[15] I. Sharifi, H. Shokrollahi, S. Amiri, Ferrite-based magnetic nanofluids used in hyperthermia applications, J. Magn. Magn. Mater. 324 (2012) 903–915.
[16] R.L. Rebodos, P.J. Vikesland, Effects of oxidation on the magnetization of nanoparticulate magnetite, Langmuir 26 (2010) 16745–16753.
[17] L. Shen, Y. Qiao, Y. Guon, S. Meng, G. Yang, M. Wu, J. Zhao, Facile coprecipitation synthesis of shape-controlled magnetite nanoparticles, Ceram. Int. 40 (2014) 1519–1524.
[18] K. Petcharoen, A. Sirivat, Synthesis and characterization of magnetite nanoparticles via the chemical co-precipitation method, Mater. Sci. Eng. B 177 (2012) 421–427.
[19] P.N. Oliveira, R.D. Bini, G.S. Dias, P. Alcouffe, I.A. Santos, L. David, L.F. Cótica, Magnetite nanoparticles with controlled sizes via thermal degradation of optimized PVA/Fe(III) complexes, J. Magn. Magn. Mater. 460 (2018) 381–390.
[20] A. Nikitin, M. Fedorova, V. Naumenko, I. Shchetinin, M. Abakumov, A. Erofeev, P. Gorelkin, G. Meshkov, E. Beloglazkina, Y. Ivanenkov, N. Klyachko, Y. Golovin, A. Savchenko, A. Majouga, Synthesis, characterization and MRI application of magnetite water-soluble cubic nanoparticles, J. Magn. Magn. Mater. 441 (2017) 6–13.
[21] Y. Bi, Y. Ren, F. Bi, T. He, Water-assisted and surfactant-free synthesis of cobalt ferrite nanospheres via solvothermal method, J. Alloy. Compd. 646 (2015) 827–832.
[22] M. Penchal Reddy, A.M.A. Mohamed, One-pot solvothermal synthesis and performance of mesoporous magnetic ferrite MFe_2O_4 nanospheres, Micropor. Mesopor. Mater. 215 (2015) 37–45.
[23] G.J. Owens, R.K. Singh, F. Foroutan, M. Alqaysi, C.-M. Han, C. Mahapatra, H.-W. Kim, J.C. Knowles, Sol–gel based materials for biomedical applications, Prog. Mater. Sci. 77 (2016) 1–79.
[24] P. Arévalo, J. Isasi, A.C. Caballero, J.F. Marco, F. Martín-Hernández, Magnetic and structural studies of Fe_3O_4 nanoparticles synthesized via coprecipitation and dispersed in different surfactants, Ceram. Int. 43 (2017) 10333–10340.
[25] P. Guardia, B. Batlle-Brugal, A.G. Roca, O. Iglesias, M.P. Morales, C.J. Serna, A. Labarta, X. Batlle, Surfactant effects in magnetite nanoparticles of controlled size, J. Magn. Magn. Mater. 316 (2007) e756–e759.
[26] P. Crespo, P. de la Presa, P. Marín, M. Multigner, J.M. Alonso, G. Rivero, F. Yndurain, J.M. González-Calbet, A. Hernando, Magnetism in nanoparticles: tuning properties with coatings, J. Phys. Condens. Matter 25 (2013) 484006.
[27] R. Regmi, V. Gumber, V. Subba Rao, I. Kohli, C. Black, C. Sudakar, P. Vaishnava, V. Naik, R. Naik, A. Mukhopadhyay, G. Lawes, Discrepancy between different estimate of the hydrodynamic diameter of polymer-coated iron oxide nanoparticles in solution, J. Nanopart. Res. 13 (2011) 6869–6875.

[28] P. Arevalo-Cid, J. Isasi, F. Martín-Hernandez, Comparative study of core–shell nanostructures based on aminofunctionalized Fe_3O_4@SiO_2 and $CoFe_2O_4$@SiO_2 nanocomposites, J. Alloy. Compd. 766 (2018) 609–618.
[29] A.M. Gutierrez, R. Bhandari, J. Weng, A. Stromberg, T.D. Dziubla, J.Z. Hilt, Novel magnetic core–shell nanoparticles for the removal of polychlorinated biphenyls from contaminated water sources, Mater. Chem. Phys. 223 (2019) 68–74.
[30] L. Alcaraz, J. Isasi, Synthesis and study of $Y_{0.9}Ln_{0.1}VO_4$ nanophosphors and $Y_{0.9}Ln_{0.1}VO_4$@SiO_2 luminescent nanocomposites with Ln = Eu, Dy, Er, Ceram. Int. 43 (2017) 5311–5318.
[31] R.D. Peterson, W. Chen, B.T. Cunningham, J.E. Andrade, Enhanced sandwich immunoassay using antibody-functionalized magnetic iron-oxide nanoparticles for extraction and detection of soluble transferrin receptor on a photonic crystal biosensor, Biosens. Bioelectron. 74 (2015) 815–822.
[32] K. Kanazaki, K. Sano, A. Makino, Y. Shimizu, F. Yamauchi, S. Ogawa, N. Ding, T. Yano, T. Temma, M. Ono, H. Saji, Development of anti-HER2 fragment antibody conjugated to iron oxide nanoparticles for in vivo HER2-targeted photoacoustic tumor imaging, Nanomed. Nanotechnol. 11 (2015) 2051–2060.
[33] I. Venugopal, S. Pernal, A. Duproz, J. Bentley, H. Engelhard, A. Linninger, Magnetic field-enhanced cellular uptake of doxorubicin loaded magnetic nanoparticles for tumor treatment, Mater. Res. Express 3 (2016) 1–13.
[34] O. Ivashchenko, A. Woźniak, E. Coy, B. Peplinska, J. Gapinski, S. Jurga, Release and cytotoxicity studies of magnetite/Ag/antibiotic nanoparticles: an interdependent relationship, Colloid. Surf. B 152 (2017) 85–94.
[35] M.D. Shultz, S. Calvin, P.P. Fatouros, S.A. Morrison, E.E. Carpenter, Enhanced ferrite nanoparticles as MRI contrast agents, J. Magn. Magn. Mater. 311 (2007) 464–468.
[36] S. Rana, A. Gallo, R.S. Srivastava, R.D.K. Misra, On the suitability of nanocrystalline ferrites as a magnetic carrier for drug delivery: functionalization, conjugation and drug release kinetics, Acta Biomater. 3 (2007) 233–242.
[37] M.G. Naseri, E.B. Saion, H.A. Ahangar, M. Hashima, A.H. Shaari, Simple preparation and characterization of nickel ferrite nanocrystals by a thermal treatment method, Powder Technol. 212 (2011) 80–88.
[38] A. Zubareva, B. Shagdarova, V. Varlamov, E. Kashirina, E. Svirshchevskaya, Penetration and toxicity of chitosan and its derivatives, Eur. Polym. J. 93 (2017) 743–749.
[39] T. Keana, M. Thanou, Biodegradation, biodistribution and toxicity of chitosan, Adv. Drug Deliv. Rev. 62 (2010) 3–11.
[40] M.N.V. Ravi, Kumar, A review of chitin and chitosan applications, React. Funct. Polym. 46 (2000) 1–27.
[41] C. Xiao, R. You, Y. Fan, Y. Zhang, Tunable functional hydrogels formed from a versatile water-soluble chitosan, Int. J. Biol. Macromol. 85 (2016) 386–390.
[42] F. Wahida, J.-J. Yin, D.-D. Xue, H. Xue, Y.-S. Lu, C. Zhong, L.-Q. Chu, Synthesis and characterization of antibacterial carboxymethyl chitosan/ZnO nanocomposite hydrogels, Int. J. Biol. Macromol. 88 (2016) 273–279.
[43] V.V. Korolev, A.G. Ramazanova, A.V. Blinov, Adsorption of surfactants on superfine magnetite, Russ. Chem. Bull. 51 (2002) 2044–2049.
[44] W. Jiang, Y. Wu, B. He, X. Zeng, K. Lai, Z. Gu, Effect of sodium oleate as a buffer on the synthesis of superparamagnetic magnetite colloids, J. Colloid Interf. Sci. 347 (2010) 1–7.
[45] H. Shagholani, S.M. Ghoreishib, M. Mousazadeh, Improvement of interaction between PVA and chitosan via magnetite nanoparticles for drug delivery application, Int. J. Biol. Macromol. 78 (2015) 130–136.
[46] A. Kaushik, P.R. Solanki, A.A. Ansari, G. Sumana, S. Ahmad, B.D. Malhotra, Iron oxide–chitosan nanobiocomposite for urea sensor, Sens. Actuators B: Chem. 138 (2009) 572–580.
[47] P.G. Jasonov, D.K. Nougaliev, B.V. Burov, F. Heller, A modernized coercivity spectrometer, Geol. Carpathica 49 (1998) 224–225.
[48] J. Isasi, P. Arévalo, E. Martín, F. Martín-Hernández, Preparation and study of silica ad APTES-silica modified $NiFe_2O_4$ nanocomposites for removal of Cu^{2+} and Zn^{2+} ions from aqueous solutions, J. Sol–Gel Sci. Techn. 43 (2019) 1–15.
[49] P. Scherrer, Bestimmung der Größe und der innerenStruktur von KolloidteilchenmittelsRöntgenstrahlen, Nachrichten von der Gesellschaft der Wissenschaftenzu Göttingen, Mathematisch-PhysikalischeKlasse 26 (1918) 98–100.
[50] F. Yazdani, M. Edrissi, Effect of pressure on the size of magnetite nanoparticles in the coprecipitation synthesis, Mater. Sci. Eng. B 171 (2010) 86–89.
[51] T. Iwasaki, K. Kosaka, N. Mizutani, S. Watano, T. Yanagida, H. Tanaka, T. Kawai, Mechanochemical preparation of magnetite nanoparticles by coprecipitation, Mater. Lett. 62 (2008) 4155–4157.
[52] K. Tao, H. Dou, K. Sun, Interfacial coprecipitation to prepare magnetite nanoparticles: concentration and temperature dependence, Colloid. Surf. A: Physicochem. Eng. Aspects 320 (2008) 115–122.
[53] M. Vadivel, R.R. Babu, M. Arivanandhan, K. Ramamurthi, Y. Hayakawa, Role of SDS surfactant concentrations on the structural, morphological, dielectric and magnetic properties of $CoFe_2O_4$ nanoparticles, RSC Adv. 5 (2015) 27060–27068.
[54] L. Zhang, R. He, H.C. Gu, Oleic acid coating on the monodisperse magnetite nanoparticles, Appl. Surf. Sci. 253 (2006) 2611–2617.
[55] K. Yang, H. Peng, Y. Wen, N. Li, Re-examination of characteristic FTIR spectrum of secondary layer in bilayer oleic acid-coated Fe_3O_4 nanoparticles, Appl. Surf. Sci. 256 (2010) 3093–3097.
[56] L. Khanna, N.K. Verma, PEG/$CaFe_2O_4$ nanocomposite: structural, morphological, magnetic and thermal analyses, Physica B 427 (2013) 68–75.
[57] J. Long, X. Yu, E. Xu, Z. Wu, X. Xu, Z. Jin, A. Jiao, In situ synthesis of new magnetite chitosan/carrageenan nanocomposites by electrostatic interactions for protein delivery applications, Carbohydr. Polym. 131 (2015) 98–107.
[58] E. Pretsch, Structure Determination of Organic Compounds, Springer, 2013.
[59] P.B. Shete, R.M. Patil, N.D. Thorat, A. Prasad, R.S. Ningthoujamb, S.J. Ghosha, S.H. Pawar, Magnetic chitosan nanocomposite for hyperthermia therapy application: preparation, characterization and in vitro experiments, Appl. Surf. Sci. 288 (2014) 149–157.
[60] J. Qu, G. Liu, Y. Wang, R. Hong, Preparation of Fe_3O_4–chitosan nanoparticles used for hyperthermia, Adv. Powder Technol. 21 (2010) 461–467.
[61] V. Pillai, D.O. Shah, Synthesis of high-coercivity cobalt ferrite particles using water-in-oil microemulsions, J. Magn. Magn. Mater. 163 (1996) 243–248.
[62] S. Mørup, E. Brok, C. Frandsen, Spin structures in magnetic nanoparticles, J. Nanomater. 2013 (2013) 720629.
[63] R.E. Morsi, A.M. Al-Sabagh, Y.M. Moustafa, S.G. El Kholy, M.S. Sayed, Polythiophene modified chitosan/magnetite nanocomposites for heavy metals and selective mercury removal, Egypt. J. Petrol. (2018), http://dx.doi.org/10.1016/j.ejpe.2018.03.004.
[64] O. Bezdorozhev, T. Kolodiazhnyi, O. Vasylkiv, Precipitation synthesis and magnetic properties of self-assembled magnetite–chitosan nanostructures, J. Magn. Magn. Mater. 428 (2017) 406–411.

[65] T.M. Freire, L.M.U. Dutra, D.C. Queiroz, N.M.P.S. Ricardo, K. Barreto, J.C. Denardin, F.R. Wurm, C.P. Sousa, A.N. Correia, P. de Lima-Neto, P.B.A. Fechine, Fast ultrasound assisted synthesis of chitosan-based magnetite nanocomposites as a modified electrode sensor, Carbohydr. Polym. 151 (2016) 760–769.

[66] R.J. Hunter, Foundations of Colloidal Science, vol. 1, Oxford Science Publications, 1986.

[67] W. Zhang, Nanoparticle aggregation: principles and modeling, Adv. Exp. Med. Biol. 811 (2014) 19–43.